Kinematic calibration of a 6-DOF hybrid robot by considering multicollinearity in the identification Jacobian

Tian Huang [a,c], Dong Zhao [a], Fuwen Yin [a], Wenjie Tian [b,*] , and Derek G. Chetwynd [c]

[a] *Key Laboratory of Mechanism Theory and Equipment Design of State Ministry of Education, Tianjin University, Tianjin 300072, China*
[b] *School of Marine Science and Technology, Tianjin University, Tianjin 300072, China*
[c] *School of Engineering, The University of Warwick, Coventry CV4 7AL, UK*

Abstract: This paper presents a systematic approach for the kinematic calibration of a 6-DOF hybrid polishing robot. It concentrates particularly on dealing with ill-conditioning that arises from multicollinearity in the identification Jacobian as a consequence of limited pose measurements. A linearized error model is formulated, using screw theory, by considering all possible source errors at the joint/link level. Calibration is based upon pose error measurements captured using a laser tracker when the polishing head undergoes pure translation within the task workspace. A two-step procedure for error parameter estimation and pose error compensation is then proposed: (1) coarse estimation and compensation of the encoder offsets using linear least squares; and (2) fine estimation of the whole set of identifiable error parameters using a Liu estimation and subsequent modification of the NC trajectory dataset of the polishing head. Both simulations and experiments on a prototype machine show that the overall standard deviation of the error parameters identified by Liu estimator is much less than that estimated by linear least squares, confirming its greater robustness in the presence of measurement uncertainty. The proposed approach results in satisfactory pose accuracy of the polishing head throughout the entire task workspace.

Keywords: Hybrid robots; Optical lens polishing; Kinematic calibration; Liu estimation

1 Introduction

Rapid developments in astronomy, space exploration and many other high-end optical instruments has created an ever increasing demand for larger, high-quality optical components. Computer Control Optimal Surfacing (CCOS), which plays an important role in optical lens polishing, achieves material removal by tuning the dwell time and relative pressure between the polishing tool and the surface being polished. Although high precision five-axis polishing machine tools have been widely used for CCOS [1], a more cost effective way to do this is to use hybrid robots [2-5] that have sufficiently high rigidity and accuracy and also offer desirable dynamic characteristics.

Geometric accuracy is one of the most important performance specifications of hybrid robots used for optical polishing. It is well known that if sufficient repeatability can be ensured *via* manufacturing and assembly processes, kinematic calibration by software is a practical and economical way to improve pose accuracy. It usually involves four successive steps: modeling, measurement, identification and compensation [6-7]. Once a complete and continuous error model is at hand, the kernel step in kinematic calibration is to estimate error parameters using a full/partial set of pose measurements that can be obtained in a cost- and time-effective manner such that inverse kinematic model residing in a controller more closely matches the real system at all possible configurations.

Large amounts of effort have been devoted over the past few decades to the geometric parameter identification of robotic mechanisms [8-11]. The methods available can be classified broadly into two categories: nonlinear and linear identification. Nonlinear identification involves estimating realistic geometric parameters or their errors by minimizing the sum of the squares of the differences between the observed poses in the given dataset and those predicted by forward kinematics. The commonly used approaches include the Newton-Gauss method [12], the Levenberg-Marquardt (L-M) algorithm [13], neural networks (NN) [14], genetic algorithms [15], and many others. However, because most geometric source errors are much smaller than their associated dimensions, the most common practice is to use linear least squares for dealing with error parameter identification of robotic mechanisms [16-20]. The procedure involves first formulating a linearized map between the pose error twist and all the possible source errors at the link/joint level. It then estimates a set of identifiable error parameters by minimizing the sum of the squares of the differences between the observed pose error twists in the given dataset and those predicted by the linearized regression model. For the purpose of pose error compensation, the ideal command dataset of the end-effector is modified by the predicted pose error twist dataset generated by the linearized error model so established. The modified command dataset of the end-effector is then converted into the joint command dataset *via* ideal inverse kinematics residing in the controller. Note that, since the pose errors caused by the encoder offsets are usually much larger than those caused by the structural errors of joints and links, it is necessary to coarsely identify and compensate the encoder offsets iteratively until they are reduced below the level at which the linearized model becomes valid for full error parameter identification and pose error compensation [21-23].

* Corresponding author
E-mail address: wenjietian@tju.edu.cn

Two important issues need to be carefully considered in error parameter identification by using linear least squares. The first issue is that the identification Jacobian, also known as the design matrix in linear regression analysis, is of perfect multicollinearity in most cases if all the possible geometric source errors at link/joint level are considered in the error modeling [24-26]. Although this problem can be tackled simply by generating a column full ranked identification Jacobian with the aid of spectral decomposition [27-28], the corresponding error parameters to be identified no longer have geometric meanings, though they are irreducible. So, the resulting estimates cannot be used for the encoder offset compensation. The second issue is of ill-conditioning arising from multicollinearity due to the limited pose measurements available in some circumstances, even when the column space of the identification Jacobian is full ranked. For example, with the hybrid polishing robot considered in this paper, the polishing head undergoes nearly pure translational motion to polish aspheric lenses having very large radii of curvature. So, in kinematic calibration of the polishing robot, it is natural and convenient to let the polishing head undergo pure translation across the task workspace in which the polishing operation will be performed. However, a preliminary study shows that some of the columns in the identification Jacobian are nearly linearly dependent due to these restricted calibration poses. This problem reduces the confidence of the error parameters estimated by linear least squares, thereby affecting the accuracy of pose error compensation at configurations different from the calibration ones. A literature review reveals that little attention has been paid to the second issue [29-30], although a number of biased estimators have been made available for dealing with multicollinearity problem of the design matrix in the field of statistics, for instance James-Stein Shrinkage Estimator (JSSE) [31], Ridge Estimator (RE) [32], Principal Components Estimator (PCE) [33], Liu Estimator (LE) [34] and many other modified versions [35-37].

Driven by the many practical needs to improve convergence rates of optical lens polishing processes, this paper presents a systematic approach for kinematic calibration of a 6-DOF hybrid polishing robot that deals particularly with the ill-conditioning problem arising from multicollinearity of the identification Jacobian. Following this introduction, Section 2 formulates a linearized error model of the polishing hybrid robot using screw theory and considering the all possible geometric source errors. In Section 3, a linear regression model is established for the relationship between the pose error twist and positional measurements of three target points on a triangle gauge. Section 4 then proposes a procedure for error parameter estimation and pose error compensation that can be implemented in two steps: (1) coarse estimation and compensation of the encoder offsets using linear least squares; and (2) fine estimation of the whole set of identifiable error parameters using a Liu estimator and modification of numerical control (NC) trajectory dataset of the polishing head. Section 5 reports both simulations and experiments on a prototype machine that show that the Liu estimator offers a more confident estimate than ordinary least squares in the fine calibration, before conclusions are drawn in Section 6.

2 Error Modeling

Fig. 1 shows a 3D view of the polishing machine being considered. It is composed essentially of a six degrees of freedom (DOF) hybrid robot, a polishing head and a magnetic worktable. The cuboid portion entailed within the reachable workspace is defined as the task workspace in which the polishing of aspheric lenses is performed. This paper concentrates on kinematic calibration of the hybrid robot in the task workspace. The hybrid robot comprises a 3-DOF parallel mechanism connected in series with a 3-DOF wrist. The parallel mechanism consists of a base, a platform, three identical UPS limbs and one properly constrained non-actuated UP limb located in the middle. The UP limb and the wrist form a UPS or UPRRR limb. Here, R, U, S and P represent, respectively, revolute, universal, spherical and prismatic joints, and the underlined P and R denote the actuated prismatic and revolute joints.

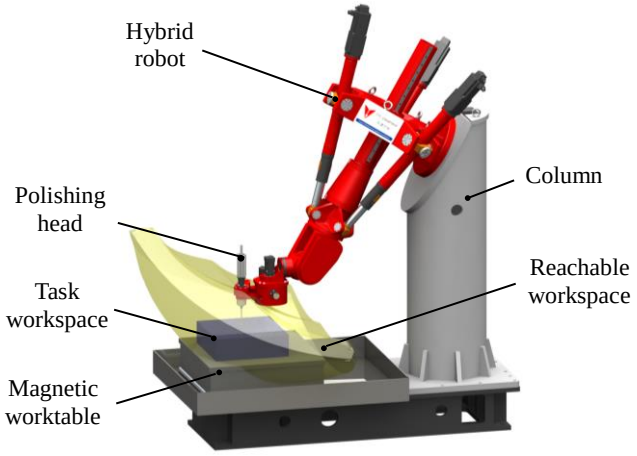

Fig. 1 3D view of the polishing robot.

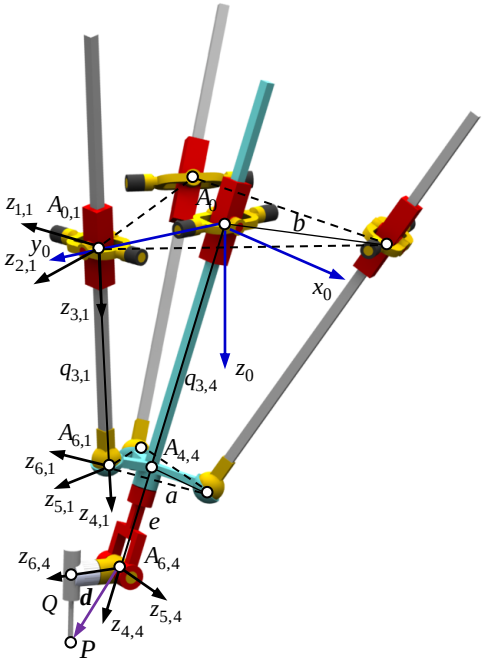

Fig. 2 Schematic diagram of the 6-DOF hybrid polishing robot.

This section uses screw theory to formulate the linear map between pose error twist of the polishing head and all possible geometric source errors in joints and links. Fig.2 shows schematic diagram of the hybrid robot. For convenience, we treat universal/spherical joints as two/three revolute joints having mutually orthogonal joint axes. We number the UPS limbs as limb 1, 2 and 3, and the UP limb plus the wrist as limb 4. In order to describe the encoder offsets and structural errors, body fixed frames $\{R_{j,i}\}$ are attached to the jth 1-DOF joint with $A_{j,i}$ as the origin and $z_{j,i}$ along the joint axis; the $x_{j,i}$ axis is the common normal to the $z_{j,i}$ and $z_{j+1,i}$ axes such that $A_{j,i}$ is the intersection of the $z_{j,i}$ and $x_{j-1,i}$ axes, except that $A_{1,i}$ is the intersection of the $z_{1,i}$ axis and the $x_{1,i}$ axis. A reference frame $\{R_0\}$ is placed on the base at the center A_0 of the ideal equilateral triangle $\Delta A_{0,1}A_{0,2}A_{0,3}$, and a floating frame $\{R_0'\}$ attached to point P with its three axes remaining parallel to those of $\{R_0\}$.

By taking P as the reference point, the pose error twist evaluated in $\{R_0'\}$ can be expressed as

$$\$_t = \$_{P,t} + \$_{S,t} \tag{1}$$

where $\$_{P,t}$ and $\$_{S,t}$ denote the 6×1 pose error twist of the parallel mechanism and that of the wrist relative to the parallel mechanism, respectively. Because all limbs in the parallel mechanism share the same platform, $\$_{P,t}$ can be written as

$$\$_{P,t} = \sum_{j=1}^{n_i} \Delta\xi_{a,j,i}\hat{\$}_{ta,j,i} + \$_{P_g,i},\ n_i = \begin{cases} 6 & i=1,2,3 \\ 3 & i=4 \end{cases} \tag{2}$$

where n_i is the connectivity of limb i; $\Delta\xi_{a,j,i}$ is the encoder offset along or about the jth joint axis and $\hat{\$}_{ta,j,i}$ the unit twist of that joint axis; and $\$_{P_g,i}$ is the pose error twist produced by the joint structural errors in the limb.

Some error sources can be separated by drawing formally on the properties of dual vector spaces [38], or *via* the physical observations that a wrench of actuations does no virtual work on a twist of constraints, and so on. Taking inner products on both sides of Eq. (2) with the unit wrench of actuations $\hat{\$}_{wa,3,i}$ imposed upon the ith UPS limb and with the unit wrench of constraints $\hat{\$}_{wc,j_c,4}$ imposed upon the UP limb, yields

$$\hat{\$}^{\mathrm{T}}_{wa,3,i}\$_{P,t} = \Delta\xi_{a,3,i} + \hat{\$}^{\mathrm{T}}_{wa,3,i}\$_{P_g,i},\ i=1,2,3 \tag{3}$$

$$\hat{\$}^{\mathrm{T}}_{wc,j_c,4}\$_{P,t} = \hat{\$}^{\mathrm{T}}_{wc,j_c,4}\$_{P_g,4},\ j_c=1,2,3 \tag{4}$$

Rewriting Eqs. (3) and (4) in matrix notation results in the error model of the parallel mechanism.

$$\$_{P,t} = \begin{bmatrix} \boldsymbol{J}_{Pa} \\ \boldsymbol{J}_{Pc} \end{bmatrix}^{-1} \left(\begin{pmatrix} \Delta\boldsymbol{\xi}_{Pa} \\ \boldsymbol{0} \end{pmatrix} + \begin{bmatrix} \boldsymbol{G}_{Pa} & \\ & \boldsymbol{G}_{Pc} \end{bmatrix} \begin{pmatrix} \Delta\boldsymbol{\eta}_{Pa} \\ \Delta\boldsymbol{\eta}_{Pc} \end{pmatrix} \right) = \boldsymbol{J}_P^{-1}\Delta\boldsymbol{\xi}_P + \boldsymbol{J}_P^{-1}\boldsymbol{G}_P\Delta\boldsymbol{\eta}_P \tag{5}$$

with

$$\boldsymbol{J}_{Pa}=\begin{bmatrix}\boldsymbol{w}_{3,1} & \boldsymbol{w}_{3,2} & \boldsymbol{w}_{3,3}\\ \boldsymbol{r}_1\times\boldsymbol{w}_{3,1} & \boldsymbol{r}_2\times\boldsymbol{w}_{3,2} & \boldsymbol{r}_3\times\boldsymbol{w}_{3,3}\end{bmatrix}^{\mathrm{T}},\ \boldsymbol{r}_i=\boldsymbol{a}_i-\boldsymbol{d}$$

$$\boldsymbol{J}_{Pc}=\begin{bmatrix}\boldsymbol{w}_{2,4} & \boldsymbol{n}_{1,4} & \boldsymbol{0}\\ \left(-\boldsymbol{d}-c\boldsymbol{w}_{3,4}\right)\times\boldsymbol{w}_{2,4} & \left(-\boldsymbol{d}-c\boldsymbol{w}_{3,4}\right)\times\boldsymbol{n}_{1,4} & \boldsymbol{n}_{3,4}\end{bmatrix}^{\mathrm{T}},\ c=q_{3,4}+e,\ \boldsymbol{n}_{1,4}=\boldsymbol{w}_{2,4}\times\boldsymbol{w}_{3,4},\ \boldsymbol{n}_{3,4}=\boldsymbol{w}_{2,4}\times\boldsymbol{w}_{1,4}$$

$$\Delta\boldsymbol{\xi}_{Pa}=\left(\Delta\xi_{a,3,1}\quad\Delta\xi_{a,3,2}\quad\Delta\xi_{a,3,3}\right)^{\mathrm{T}}=\left(\Delta q_1\quad\Delta q_2\quad\Delta q_3\right)^{\mathrm{T}}$$

$$\boldsymbol{G}_{Pa}\Delta\boldsymbol{\eta}_{Pa}=\begin{pmatrix}\hat{\$}_{wa,3,1}^{\mathrm{T}}\$_{p_g,1}\\ \hat{\$}_{wa,3,2}^{\mathrm{T}}\$_{p_g,2}\\ \hat{\$}_{wa,3,3}^{\mathrm{T}}\$_{p_g,3}\end{pmatrix},\ \boldsymbol{G}_{Pc}\Delta\boldsymbol{\eta}_{Pc}=\begin{pmatrix}\hat{\$}_{wc,1,4}^{\mathrm{T}}\$_{p_g,4}\\ \hat{\$}_{wc,2,4}^{\mathrm{T}}\$_{p_g,4}\\ \hat{\$}_{wc,3,4}^{\mathrm{T}}\$_{p_g,4}\end{pmatrix}$$

where $\boldsymbol{w}_{j,i}$ is the 3×1 nominal unit vector of the jth joint axis, Δq_i is the encoder offset of the P joint in the ith UPS limb; $\Delta\boldsymbol{\eta}_{Pa}$ and $\Delta\boldsymbol{\eta}_{Pc}$ are the joint structural error vectors of the UPS limbs and the UP limb; $\boldsymbol{r}_i$ is the 3×1 nominal position vector pointing from P to $A_{6,i}$ with $\boldsymbol{d}=\overrightarrow{A_{6,4}P}$ and $\boldsymbol{a}_i=\overrightarrow{A_{6,4}A_{6,i}}$; c is the nominal length from A_0 to $A_{6,4}$ with $q_{3,4}=\left\|\overrightarrow{A_0A_{4,4}}\right\|$ and $e=\left\|\overrightarrow{A_{4,4}A_{6,4}}\right\|$. For the derivation of $\$_{p_g,i}$ in terms of the corresponding source errors, please see Appendix A.

A similar technique formulates the pose error twist of the wrist relative to the parallel mechanism as

$$\$_{S,t}=\sum_{j=4}^{6}\Delta\xi_{a,j,4}\hat{\$}_{ta,j,4}+\$_{S_g}=\boldsymbol{J}_S\Delta\boldsymbol{\xi}_S+\boldsymbol{G}_S\Delta\boldsymbol{\eta}_S \tag{6}$$

with

$$\boldsymbol{J}_S=\begin{bmatrix}-\boldsymbol{d}\times\boldsymbol{w}_{4,4} & -\boldsymbol{d}\times\boldsymbol{w}_{5,4} & -\boldsymbol{d}\times\boldsymbol{w}_{6,4}\\ \boldsymbol{w}_{4,4} & \boldsymbol{w}_{5,4} & \boldsymbol{w}_{6,4}\end{bmatrix}$$

$$\Delta\boldsymbol{\xi}_S=\left(\Delta\xi_{a,4,4}\quad\Delta\xi_{a,5,4}\quad\Delta\xi_{a,6,4}\right)^{\mathrm{T}}=\left(\Delta\theta_4\quad\Delta\theta_5\quad\Delta\theta_6\right)^{\mathrm{T}}$$

where $\Delta\xi_{a,j,4}=\Delta\theta_j$ and $\hat{\$}_{ta,j,4}$ are the encoder offset about the jth (j=4,5,6) actuated joint axis and the nominal unit twist of that joint axis of the wrist; and $\$_{S_g}$ is the pose error twist produced by the joint structural errors of the wrist. For the formulation of $\$_{S_g}$ in terms of the corresponding source errors, please again refer to Appendix A.

Substituting Eqs. (5) and (6) into Eq. (1) leads to the linear map between the error parameter vector $\Delta\boldsymbol{\chi}$ and the pose error twist $\$_t$ of the polishing head:

$$\$_t=\boldsymbol{B}\Delta\boldsymbol{\chi} \tag{7}$$

where

$$\Delta\boldsymbol{\chi}=\begin{pmatrix}\Delta\boldsymbol{\xi}\\ \Delta\boldsymbol{\eta}\end{pmatrix},\ \Delta\boldsymbol{\xi}=\begin{pmatrix}\Delta\boldsymbol{\xi}_P\\ \Delta\boldsymbol{\xi}_S\end{pmatrix},\ \Delta\boldsymbol{\eta}=\begin{pmatrix}\Delta\boldsymbol{\eta}_P\\ \Delta\boldsymbol{\eta}_S\end{pmatrix}$$

$$\boldsymbol{B}=\begin{bmatrix}\boldsymbol{B}_\xi & \boldsymbol{B}_\eta\end{bmatrix},\ \boldsymbol{B}_\xi=\begin{bmatrix}\boldsymbol{J}_P^{-1} & \\ & \boldsymbol{J}_S\end{bmatrix},\ \boldsymbol{B}_\eta=\begin{bmatrix}\boldsymbol{J}_P^{-1}\boldsymbol{G}_P & \\ & \boldsymbol{G}_S\end{bmatrix}$$

For practical use, the pose accuracy should be expressed in the workpiece frame $\{R\}$ having its z axis normal to the worktable and its y axis parallel to x_0, as shown in Fig. 3. The pose error twist evaluated in $\{R\}$ can be obtained by the simple adjoint transformation comprising two successive elementary rotations, giving

$${}^{w}\$_t={}^{w}\boldsymbol{A}_0\,{}^{0}\$_t={}^{w}\boldsymbol{A}_0\boldsymbol{B}\Delta\boldsymbol{\chi} \tag{8}$$

with

$${}^{w}\boldsymbol{A}_0=\begin{bmatrix}{}^{w}\boldsymbol{R}_0 & \boldsymbol{0}\\ \boldsymbol{0} & {}^{w}\boldsymbol{R}_0\end{bmatrix},\ {}^{w}\boldsymbol{R}_0=\mathrm{Rot}\left(y,\pi-\beta\right)\mathrm{Rot}\left(z,0.5\pi\right)$$

where ${}^{0}\$_t=\$_t$ as given in Eq. (7) and β is the nominal structural angle between the z and z_0 axes. For the robot considered here, $\beta=\pi/6$. Hereafter, because this transformation is fixed and can be implied, we will denote ${}^{w}\$_t$ as $\$_t$ and ${}^{w}\boldsymbol{A}_0\boldsymbol{B}$ as $\boldsymbol{B}$ for simplicity unless indicated otherwise.

3 Pose Error Measurement

The error model given by Eq. (8) enables the formulation of a measurement scheme and linear regression model for error parameter identification. As shown in Fig. 3(a), the workpiece frame $\{R\}$ is placed with its x and y axes parallel to two orthogonal edges of the magnetic worktable. The reference pose is defined to be when P is coincident with the center of the cubic task workspace, the nominal $z_{5,4}$ axis is coincident with the y axis, and the nominal $z_{6,4}$ axis is coincident with the x axis of $\{R\}$. To facilitate the pose error measurement of the polishing head using a laser tracker, three target points, sequentially denoted by P_1, P_2 and P_3, are seated on an isosceles triangular gauge that is rigidly mounted on the polishing head such that $\Delta P_1P_2P_3 \perp \overline{P_0P}$ and $\overline{P_0P_1} \perp \overline{P_2P_3}$, with $\overline{P_2P_3}$ and $\overline{P_0P_1}$ set as nearly parallel as possible to the x and y axes at the reference pose.

The cuboid task space is divided into n_c layers, each nominally parallel to xy, and the polishing head undergoes nominally pure translation in each calibration layer while the coordinates of each target point with respect to $\{R\}$ are captured by a laser tracker at $L\times L$ evenly spaced nodes, see Fig. 3(b). The proposed calibration pose arrangement considers two important factors: (1) the polishing head need only undergo nearly translational motion throughout the task workspace due to the small curvatures of the aspheric lenses being polished; (2) all active joints are actuated simultaneously to fulfill the requirement for $\Delta\boldsymbol{\xi}$ to be identifiable using a minimum set of pose measurements [39]. Denoting the position coordinates of the gauge targets at the kth calibration node as $P_{j,k}$ ($j=1,2,3$), a linear map between $\$_{t,k}$, the pose error twist of P_k, and the corresponding position errors of the three target points is

$$\Delta\boldsymbol{p}_k = \boldsymbol{P}_k \$_{t,k},\ k=1,2,\ldots,n_cL^2 \tag{9}$$

$$\Delta\boldsymbol{p}_k = \begin{pmatrix} \boldsymbol{p}_{1,k}-\boldsymbol{p}_{01,k} \\ \boldsymbol{p}_{2,k}-\boldsymbol{p}_{02,k} \\ \boldsymbol{p}_{3,k}-\boldsymbol{p}_{013k} \end{pmatrix} = \begin{pmatrix} \Delta\boldsymbol{p}_{1,k} \\ \Delta\boldsymbol{p}_{2,k} \\ \Delta\boldsymbol{p}_{3,k} \end{pmatrix},\ \boldsymbol{P}_k = \begin{bmatrix} \boldsymbol{P}_{1,k} \\ \boldsymbol{P}_{2,k} \\ \boldsymbol{P}_{3,k} \end{bmatrix},\ \boldsymbol{P}_{j,k} = \begin{bmatrix} \boldsymbol{I}_3 & \left[\hat{\boldsymbol{p}}_{j,k}\times\right] \end{bmatrix},\ \$_{t,k} = \begin{pmatrix} \Delta\boldsymbol{p}_{0,k} \\ \Delta\boldsymbol{\theta}_k \end{pmatrix}$$

where $\Delta\boldsymbol{p}_{0,k}$ and $\Delta\boldsymbol{\theta}_k$ are the 3×1 position error vector of P_k and the orientation error vector of the polishing head at the kth calibration pose; $\boldsymbol{p}_{j,k}$ and $\boldsymbol{p}_{0\,j,k}$ ($j=1,2,3$) are the measured and nominal position vectors of $P_{j,k}$; $\left[\hat{\boldsymbol{p}}_{j,k}\times\right]$ is the skew matrix of $\hat{\boldsymbol{p}}_{j,k}$, representing the cross product with the nominal position vector pointing from $P_{j,k}$ to P_k at the same configuration; and $\boldsymbol{I}_3$ denotes a 3×3 identity matrix.

Substituting the pose error twist model given by Eq. (8) into Eq. (9) and rewriting in matrix form, finally results in the linear regression model

$$\Delta\boldsymbol{p} = \boldsymbol{H}\Delta\boldsymbol{\chi} + \boldsymbol{\varepsilon} \tag{10}$$

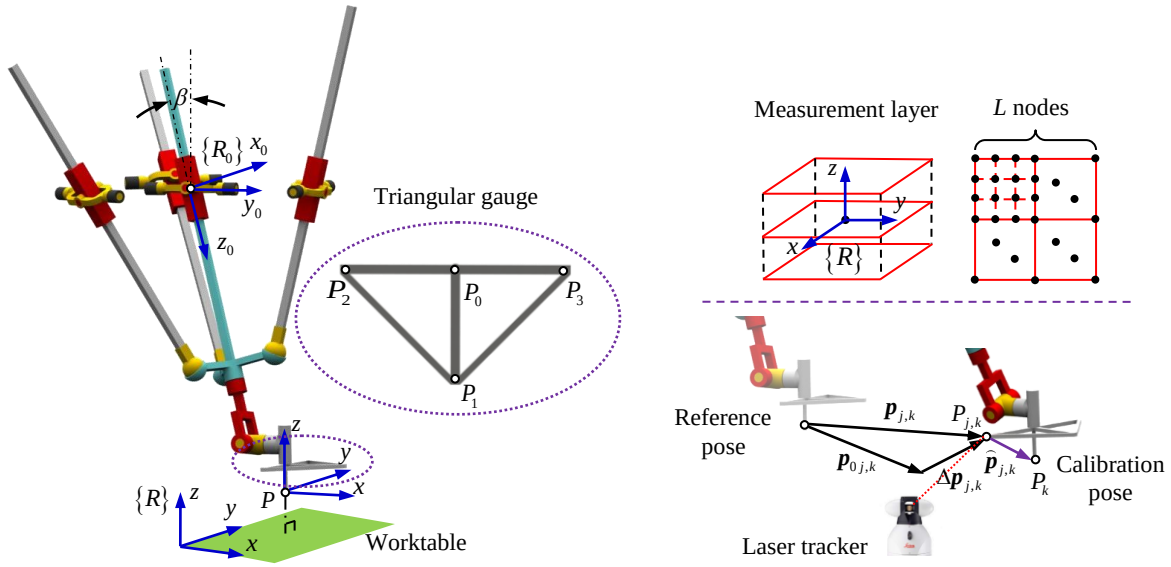

(a) Establishment of the $\{R\}$ (b) Pose error measurement

Fig. 3 Pose error measurement of the polishing robot.

$$\Delta \boldsymbol{p} = \begin{pmatrix} \Delta \boldsymbol{p}_1 \\ \vdots \\ \Delta \boldsymbol{p}_{n_c L^2} \end{pmatrix}, \quad \boldsymbol{H} = \begin{bmatrix} \boldsymbol{P}_1 \boldsymbol{B}_1 \\ \vdots \\ \boldsymbol{P}_{n_c L^2} \boldsymbol{B}_{n_c L^2} \end{bmatrix}$$

where $\boldsymbol{H}$ denotes a $n \times m$ matrix known as the identification Jacobian, $\boldsymbol{\varepsilon}$ is an $n \times 1$ residual error vector assumed to have a normal distribution, $n = 9 n_c L^2$ and $m = \dim(\Delta \boldsymbol{\chi})$.

4 Error Parameter Estimation and Pose Error Compensation

Having the linear regression model given by Eq. (10), a systematic procedure is developed in this section to estimate error parameters and compensate pose errors *via* three successive steps.

4.1 Reconstruction of the identification Jacobian

The necessary condition for $\Delta \boldsymbol{\chi}$ to be identifiable is that column space of $\boldsymbol{H}$ must be full ranked [40]. In practice, however, this requirement is not fulfilled in the majority of cases generally and not for the hybrid polishing robot in particular. This critical problem can be dealt with by either of two ways.

The first way is to generate a column full ranked identification Jacobian $\boldsymbol{Z}_1 = \boldsymbol{H} \boldsymbol{\Phi}_1$ by spectral decomposition such that $\Delta \boldsymbol{\chi} = \boldsymbol{\Phi}_1 \Delta \boldsymbol{\alpha}$ where $\boldsymbol{\Phi}_1$ is a block matrix formed by the eigenvectors corresponding to the non-zero eigenvalues of $\boldsymbol{H}^{\mathrm{T}} \boldsymbol{H}$. This leads to a modified linear regression model $\Delta \boldsymbol{p} = \boldsymbol{Z}_1 \Delta \boldsymbol{\alpha} + \boldsymbol{\varepsilon}$ where $\operatorname{rank}\left(\boldsymbol{Z}_1^{\mathrm{T}} \boldsymbol{Z}_1\right) = \dim(\Delta \boldsymbol{\alpha}) = m_1$. For convenience, we continue to denote $\Delta \boldsymbol{\alpha}$, $\boldsymbol{Z}_1$ and m_1 as $\Delta \boldsymbol{\chi}$, $\boldsymbol{H}$ and m (i.e., assuming such corrections have been made) unless indicated otherwise.

The second way is to reconstruct a column full ranked identification Jacobian by correlation analysis of $\boldsymbol{H} = \begin{bmatrix} \boldsymbol{H}_\xi & \boldsymbol{H}_\eta \end{bmatrix}$ where $\boldsymbol{H}_\xi$ and $\boldsymbol{H}_\eta$ are block matrices associated respectively with $\Delta \boldsymbol{\xi}$ and $\Delta \boldsymbol{\eta}$, as defined at Eq. (7). Note that $\dim(\Delta \boldsymbol{\xi}) = f$ and $\dim(\Delta \boldsymbol{\eta}) = m - f$ where f is the number of the actuated joints. Since $\operatorname{rank}\left(\boldsymbol{H}_\xi\right) = f$ is always ensured at nonsingular configurations, a simple and straightforward algorithm of the reconstruction is proposed:

Step 1: Let $\boldsymbol{h}_{\eta,j}$ be the jth ($j = 1, 2, \cdots, m - f$) column vector of $\boldsymbol{H}_\eta$ and let $\boldsymbol{H}_\xi$ be the initial $\boldsymbol{H}$;

Step 2: For every j, if $\operatorname{rank}\left(\begin{bmatrix} \boldsymbol{H} & \boldsymbol{h}_{\eta,j} \end{bmatrix}\right) = \operatorname{rank}(\boldsymbol{H}) + 1$, then $\boldsymbol{H} = \begin{bmatrix} \boldsymbol{H} & \boldsymbol{h}_{\eta,j} \end{bmatrix}$. Otherwise, $\boldsymbol{H}$ remains unchanged;

Step 3: Let $m = \operatorname{rank}(\boldsymbol{H})$ and reconstruct $\boldsymbol{B}_\eta$ in Eqs. (7) and (8) accordingly.

An obvious advantage of the second approach is that the reconstructed $\boldsymbol{H}$ remains in the form $\boldsymbol{H} = \begin{bmatrix} \boldsymbol{H}_\xi & \boldsymbol{H}_\eta \end{bmatrix}$ such that a coarse calibration can be carried out by first identifying and compensating $\Delta \boldsymbol{\xi}$ iteratively until the norm of its relative change is reduced below the level at which the linearized regression model becomes valid for estimating $\Delta \boldsymbol{\chi}$. In addition, note that $\boldsymbol{H}$ reconstructed by either of two approaches is not unique, leading to a non-unique estimate for $\Delta \boldsymbol{\chi}$. However, this non-uniqueness does not affect the final results of pose error compensation because $\Delta \boldsymbol{\chi}$ will be estimated in such a way that enables the overall discrepancy between the predicted and observed pose errors to be minimized in a sense of least squares.

4.2 Error parameter estimation

As discussed in Section 3, it is convenient to let the polishing head undergo pure translation in the calibration pose measurement in order to avoid potential interruption of the laser beam. However, this restricted range of calibration poses may lead to problems of ill-conditioning arising from multicollinearity of the identification Jacobian, even though the column space of $\boldsymbol{H}$ is now assumed to be full ranked. Mathematically, so-called multicollinearity means that at least two columns of $\boldsymbol{H}$ are nearly linearly dependent. If so, $\Delta \boldsymbol{\chi}$ estimated by ordinary least squares (OLS) becomes very sensitive to measurement disturbance [40], which in turn affects the quality of pose error compensation at configurations that differ from the calibration ones.

Liu-type estimators [34-37] are especially designed for dealing with multicollinearity of the identification Jacobian. This article employs the Liu estimator (LE) proposed in [34] to estimate the whole set of identifiable error parameters. LE is an improved version of OLS, featuring a single biasing parameter for modifying the regression coefficients *via* relaxing unbiasedness. For the particular problem, the estimate for $\Delta \boldsymbol{\chi}$ can be expressed as

$$\Delta \hat{\boldsymbol{\chi}}_L = \left(\boldsymbol{H}^{\mathrm{T}} \boldsymbol{H} + \boldsymbol{I}_m\right)^{-1} \left(\boldsymbol{H}^{\mathrm{T}} \Delta \boldsymbol{p} + d \Delta \hat{\boldsymbol{\chi}}\right) \tag{11}$$

where subscript L indicates a Liu estimation, $\boldsymbol{I}_m$ is an $m \times m$ identity matrix and $0 < d < 1$ is a biasing parameter known as the Liu parameter which can be determined by the following process.

In the light of spectral decomposition, let

$$\boldsymbol{Z}=\boldsymbol{H}\boldsymbol{\Phi},\ \Delta\boldsymbol{\alpha}=\boldsymbol{\Phi}^{\mathrm{T}}\Delta\boldsymbol{\chi}\ \text{ with }\ \boldsymbol{Z}^{\mathrm{T}}\boldsymbol{Z}=\boldsymbol{\Lambda}=\mathrm{diag}\left(\lambda_j\right) \tag{12}$$

where $\boldsymbol{\Lambda}=\mathrm{diag}\left(\lambda_j\right)$ is a diagonal matrix formed by the eigenvalues and $\boldsymbol{\Phi}$ is an orthogonal matrix formed by the corresponding eigenvectors of $\boldsymbol{H}^{\mathrm{T}}\boldsymbol{H}$. It has been proved [34] that the mean square error of $\Delta\hat{\boldsymbol{\alpha}}_L$ for $\Delta\boldsymbol{\alpha}$ has the form

$$\mathrm{MSE}\left(\Delta\hat{\boldsymbol{\alpha}}_L\right)=\hat{\sigma}^2\sum_{j=1}^{m}\frac{\left(\lambda_j+d\right)^2}{\lambda_j\left(\lambda_j+1\right)^2}+\left(d-1\right)^2\sum_{j=1}^{m}\frac{\Delta\hat{\alpha}_j^2}{\left(\lambda_j+1\right)^2} \tag{13}$$

where

$$\hat{\sigma}^2=\frac{1}{n}\mathrm{tr}\left[\left(\Delta\boldsymbol{p}-\boldsymbol{H}\Delta\hat{\boldsymbol{\chi}}\right)\left(\Delta\boldsymbol{p}-\boldsymbol{H}\Delta\hat{\boldsymbol{\chi}}\right)^{\mathrm{T}}\right],\ \Delta\hat{\alpha}_j^2=\left(\boldsymbol{\Phi}^{\mathrm{T}}\Delta\hat{\boldsymbol{\chi}}\Delta\hat{\boldsymbol{\chi}}^{\mathrm{T}}\boldsymbol{\Phi}\right)_{jj}$$

Then, the Liu parameter d can be obtained explicitly by minimizing $\mathrm{MSE}\left(\Delta\hat{\boldsymbol{\alpha}}_L\right)$, which is equivalent to minimizing $\mathrm{MSE}\left(\Delta\hat{\boldsymbol{\chi}}_L\right)$ because $\Delta\hat{\boldsymbol{\chi}}=\boldsymbol{\Phi}\Delta\hat{\boldsymbol{\alpha}}$. Hence,

$$d=\sum_{i=1}^{m}\frac{\Delta\hat{\alpha}_i^2-\hat{\sigma}^2}{\left(\lambda_i+1\right)^2}\Bigg/\sum_{i=1}^{m}\frac{\hat{\sigma}^2+\lambda_i\Delta\hat{\alpha}_i^2}{\lambda_i\left(\lambda_i+1\right)^2} \tag{14}$$

4.3 Pose error compensation

With a column full ranked identification Jacobian to hand, kinematic calibration of the polishing hybrid robot can be implemented by successive coarse and fine calibrations. For the coarse calibration, the pose error twist induced by $\Delta\boldsymbol{\eta}$ is treated as an additional 'measurement disturbance'. This allows $\Delta\boldsymbol{\xi}$ to be roughly estimated by OLS, requiring an iterative process because of the cut-off errors of linearization. The estimate after each iteration updates its nominal one until the relative change between two successive estimates is below a specified threshold, that is

$$\hat{\boldsymbol{\xi}}^{k+1}=\hat{\boldsymbol{\xi}}^{k}+\Delta\hat{\boldsymbol{\xi}}^{k}\ \text{ until }\left(\frac{\left\|\Delta\hat{\boldsymbol{\xi}}^{k+1}-\Delta\hat{\boldsymbol{\xi}}^{k}\right\|}{\left\|\Delta\hat{\boldsymbol{\xi}}^{k}\right\|}\right)\le\varepsilon_{\xi}\ \text{ with }\ \Delta\hat{\boldsymbol{\xi}}^{k}=\left(\boldsymbol{H}_{\xi}^{\mathrm{T}}\boldsymbol{H}_{\xi}\right)^{-1}\boldsymbol{H}_{\xi}^{\mathrm{T}}\Delta\boldsymbol{p}^{k} \tag{15}$$

where $\hat{\boldsymbol{\xi}}^{k}$ and $\Delta\boldsymbol{p}^{k}$ denote the initial encode setting vector and the measured pose error vector in the kth round of coarse calibration; and ε_{ξ} denotes the specified threshold. It should be noted that the number of calibration nodes required for coarse calibration is much fewer than is required in the fine calibration because only $\Delta\boldsymbol{\xi}$ needs to be identified.

Note that it is difficult, if not impossible, to formulate an inverse kinematic model that contains all error parameters and to compensate pose error by correcting these parameters. So, starting with a satisfactory coarse calibration, the fine calibration is carried out by identifying $\Delta\boldsymbol{\chi}$ using LE and storing the estimate $\Delta\hat{\boldsymbol{\chi}}_L$ in the master computer of a CNC system. For the purpose of pose error compensation, the dataset of the polishing head created *via* rough interpolation of the nominal NC code is modified by the predicted pose error dataset generated using the same interpolation period, i.e.

$$\left\{\$_f\right\}=\left\{\$_{f0}\right\}-\left\{\$_t\right\},\ \$_t=\boldsymbol{B}\Delta\hat{\boldsymbol{\chi}}_L \tag{16}$$

where $\left\{\$_{f0}\right\}$ and $\left\{\$_t\right\}$ are the nominal pose dataset and the predicted pose error dataset. Then $\left\{\$_f\right\}$ can be converted into the command dataset of the actuated joints $\boldsymbol{\xi}_m$ *via* the ideal inverse kinematics of the polishing robot. Fig. 4 shows the flowchart of the proposed two-step strategy for pose error compensation, where symbol F^{-1} represents the ideal inverse displacement analysis.

5 Verification

Both simulations and experiments have been carried out on a hybrid polishing robot (see Fig. 5) to verify the effectiveness of the proposed calibration method. Particular interest is given here to examining the capability of LE over OLS in dealing with multicollinearity of the identification Jacobian. The nominal dimensions of the test robot are given in Table 1, resulting in a cuboid task workspace of $500\ \mathrm{mm}\times500\ \mathrm{mm}\times120\ \mathrm{mm}$. It uses a CNC system built upon an IPC + PMAC open architecture.

Position data measurements for the calibration process used a LEICA AT901-LR laser tracker with the maximum observed deviation of 0.005 mm/m. As shown in Fig. 5, the workpiece frame $\{R\}$ defined in Section 3 is established using the position data of three target points (the center of a sphere reflector) on a square gauge located at a corner of the magnetic worktable. Then the polishing head is moved to the reference pose defined in Section 3 *via* JOG operations and the encoder settings initialized. Prior to kinematic calibration, a repeatability test was conducted according to ISO9283 [42]. Each measurement was repeated thirty times and the mean value retained. The results showed that a volumetric position repeatability of 0.016 mm and a volumetric orientation repeatability of 0.010 deg can be achieved within the cuboid task workspace. For the coarse calibration, the polishing head was commanded to undergo pure translation through

Table 1 Nominal dimensions of the hybrid robot (unit: mm).

$\left\|\overrightarrow{A_{0,i}A_{1,i}}\right\|$	$\left\|\overrightarrow{A_{4,4}A_{6,4}}\right\|$	$\left\|\overrightarrow{A_{4,4}A_{6,i}}\right\|$	$\left\|\overrightarrow{A_{6,4}Q}\right\|$	$\left\|\overrightarrow{QP_0}\right\|$	$\left\|\overrightarrow{P_0P}\right\|$	$\left\|\overrightarrow{P_0P_i}\right\|$	$q_{\min}$	$q_{\max}$
350	345	135	405	120	250	200	628	1178

$q_{\min}$ and $q_{\max}$ denote the minimum and maximum lengths of the UPS limbs

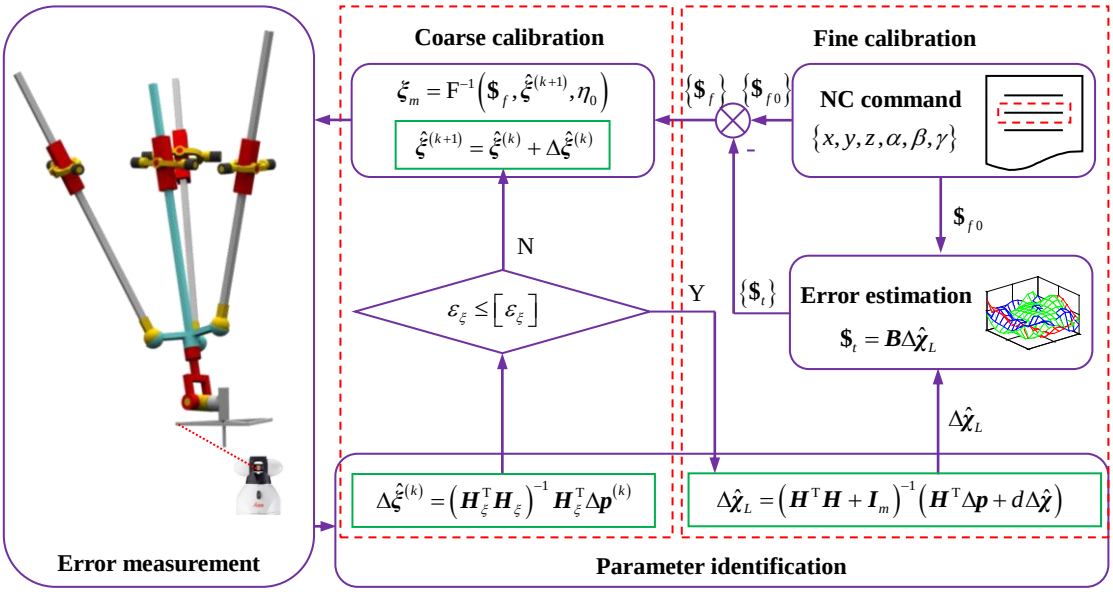

Fig. 4 The hierarchical strategy for error compensation.

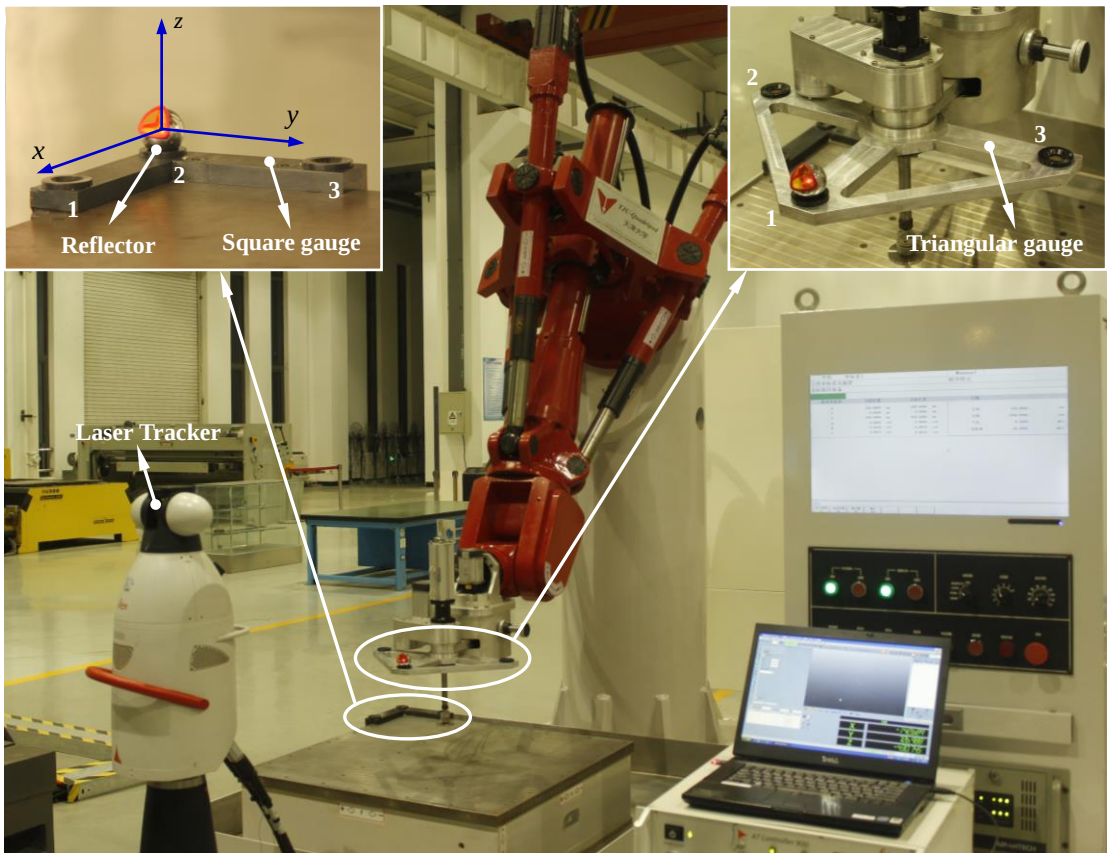

Fig. 5 Experiment set-up for kinematic calibration of the hybrid polishing robot.

$L \times L = 5 \times 5 = 25$ nodes evenly spaced in the calibration layer (the middle layer) of the task workspace, resulting in $n = 9 \times 25 = 225$ pose error measurements from the position data of three target points seated on the triangular gauge shown in Fig. 5. The positional accuracy of the target point seats relative to P was tested by a CMM for precisely determining the positioning vector pointing from P_j to P. The measurement at each calibration pose was repeated three times and the mean value retained. Then, $\Delta\boldsymbol{\xi}$ was estimated by OLS using the pose error dataset measured in the calibration layer and that estimate used to update the initial encoder settings until the relative change (see Eq. (15)) was below a threshold of $\varepsilon_\xi = 5\%$. In order to examine the results of the coarse calibration, the pose error twist at each node in the calibration layer (the middle layer) and those in two test layers (the upper layer and the lower layer) were measured after the coarse calibration. Interpolated by cubic splines, Fig. 6 and Fig. 7 show the volumetric position and orientation error distributions of the polishing head in the calibration layer and one of the test layers (the lower layer). It can be seen that the $\Delta\hat{\boldsymbol{\xi}}$ estimated by OLS works well in predicting the pose errors in both calibration and test layers thanks to the well-conditioned $\boldsymbol{H}_\xi$. This enables the maximum value of the position and orientation pose errors to be held below 0.170 mm and 0.210 deg after the coarse calibrations.

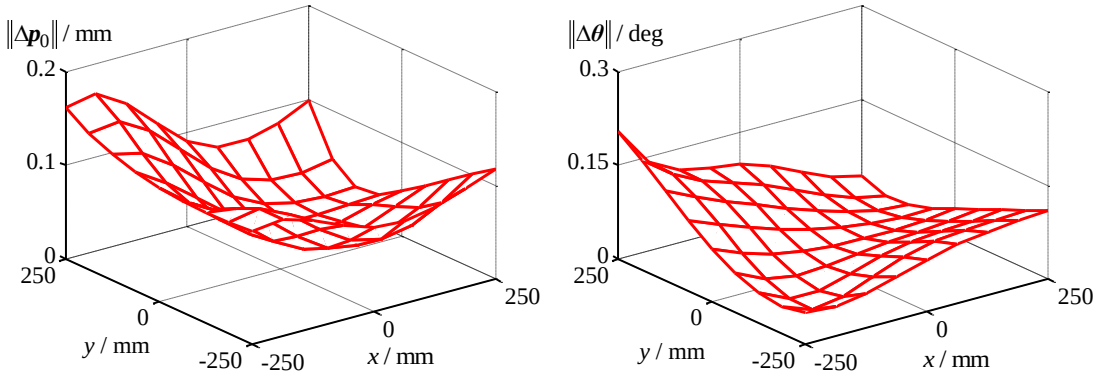

(a) (b)

Fig. 6 Pose error distributions in the calibration (middle) layer after the coarse calibration (a) position error (b) orientation error.

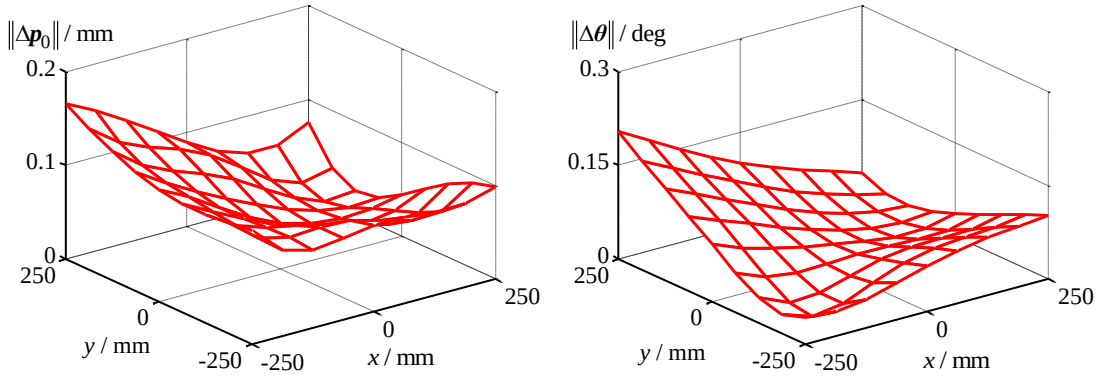

(a) (b)

Fig. 7 Pose error distributions in the test (lower) layer after the coarse calibration (a) position error (b) orientation error.

Before considering fine calibration, it is necessary to examine *via* simulation the robustness of the whole set of identifiable error parameters estimated by OLS and by LE. So, a skeleton CAD model of the robot has been built using SolidWorks, in which the all possible source errors are taken into account in such a way that their values match exactly those in the error model established in Section 2. This CAD model was used to simulate the measured pose errors by adding 'measurement disturbance' in a Monte Carlo study. For the simulation, $\boldsymbol{H}$ was reconstructed by the second method proposed in Section 4.1, resulting in 54 irreducible error parameters (see Table 2) out of 145 source errors. Here, we still use the symbolic notations in the Section 2 to denote the reduced parameters for simplicity. It can be seen from that limbs 2 and 3 have the same irreducible parameters because the two limbs and the chosen measurement nodes share the same symmetry plane. White noise with standard deviation of 0.005 mm was added to position error data points to simulate the

Table 2 A set of irreducible parameters

Limb	$\Delta\boldsymbol{\xi}$	$\Delta\boldsymbol{\eta}_{0,i}$	$\Delta\boldsymbol{\eta}_{1,i}$	$\Delta\boldsymbol{\eta}_{2,i}$
1	$\Delta\xi_{a,3,1}$	$\Delta x_{0,1}, \Delta y_{0,1}, \Delta z_{0,1}$	N/A	$\Delta x_{2,1}, \Delta z_{2,1}$
2	$\Delta\xi_{a,3,2}$	$\Delta x_{0,2}, \Delta y_{0,2}, \Delta z_{0,2}$	N/A	$\Delta x_{2,2}, \Delta z_{2,2}$
3	$\Delta\xi_{a,3,3}$	$\Delta x_{0,3}, \Delta y_{0,3}, \Delta z_{0,3}$	N/A	$\Delta x_{2,3}, \Delta z_{2,3}$
4	$\Delta\xi_{a,4,4}, \Delta\xi_{a,5,4}, \Delta\xi_{a,6,4}$,	$\Delta\boldsymbol{\eta}_{0,4}$	N/A	$\Delta x_{2,4}, \Delta z_{2,4}, \Delta\alpha_{2,4}$
Limb	$\Delta\boldsymbol{\eta}_{3,i}$	$\Delta\boldsymbol{\eta}_{4,i}$	$\Delta\boldsymbol{\eta}_{5,i}$	$\Delta\boldsymbol{\eta}_{6,i}$
1	$\Delta z_{3,1}, \Delta\alpha_{3,1}$	N/A	N/A	N/A
2	$\Delta z_{3,2}, \Delta\alpha_{3,2}$	N/A	N/A	$\Delta x_{6,2}, \Delta z_{6,2}$
3	$\Delta z_{3,3}, \Delta\alpha_{3,3}$	N/A	N/A	$\Delta x_{6,3}, \Delta z_{6,3}$
4	$\Delta x_{3,4}, \Delta z_{3,4}, \Delta\alpha_{3,4}, \Delta\beta_{3,4}$	$\Delta\boldsymbol{\eta}_{4,4}$	$\Delta x_{5,4}, \Delta z_{5,4}, \Delta\alpha_{5,4}$	$\Delta y_{6,4}, \Delta\alpha_{6,4}$

measurement disturbance. $\Delta\boldsymbol{\chi}$ was estimated repeatedly over 10^4 runs by each of OLS and LE, using the simulated pose errors 'measured' at $L\times L = 7\times 7 = 49$ evenly spaced nodes in each of two calibration layers (the upper and lower layers) of the task workspace. The relative robustness of two estimators against 'measurement disturbance' could then be evaluated by the index (reduction in stability against noise)

$$\eta = \left(1 - \frac{\sigma\left(\Delta\hat{\boldsymbol{\chi}}_L\right)}{\sigma\left(\Delta\hat{\boldsymbol{\chi}}\right)}\right)\times 100\% \tag{17}$$

with

$$\sigma\left(\Delta\hat{\boldsymbol{\chi}}\right) = \sqrt{\sum_{i=1}^{m} D\left(\Delta\hat{\chi}_i\right)}\ ,\ \sigma\left(\Delta\hat{\boldsymbol{\chi}}_L\right) = \sqrt{\sum_{i=1}^{m} D\left(\Delta\hat{\chi}_{L,i}\right)} \tag{18}$$

where $\sigma\left(\Delta\hat{\boldsymbol{\chi}}\right)$ is defined as the overall standard deviation of $\Delta\hat{\boldsymbol{\chi}}$ estimated by OLS, and $\sigma\left(\Delta\hat{\boldsymbol{\chi}}_L\right)$ is that of $\Delta\hat{\boldsymbol{\chi}}_L$ estimated by LE; $D\left(\Delta\hat{\chi}_i\right)$ and $D\left(\Delta\hat{\chi}_{L,i}\right)$ denote the standard deviation of the *i*th error parameter in $\Delta\hat{\boldsymbol{\chi}}$ and $\Delta\hat{\boldsymbol{\chi}}_L$, respectively. The simulation resulted in $\eta = 63.9\ \%$ for this particular problem, meaning that LE is indeed workable in dealing with the ill-conditioning arising from multicollinearity of the identification Jacobian.

With the simulation providing confidence in the LE process and the coarse calibration completed, the fine calibration was carried out using the procedure addressed in Section 4.3, because the linearized regression model was then valid for estimating $\Delta\boldsymbol{\chi}$. For the fine calibration, the upper and lower layers were used as the calibration layers, while the middle layer was taken as the test layer. As shown in Tables 3 and 4, $\Delta\boldsymbol{\chi}$ was estimated by both OLS and LE using the position error data measured at $L\times L = 7\times 7 = 49$ evenly spaced nodes in each of the two calibration layers. Pose error compensation was performed according to Eq. (16). Fig. 8 and Fig. 9 show the volumetric position and orientation error distributions of the polishing head in one of the calibration layers (the lower layer) and in the test layer. They show that following coarse calibration, the overall pose accuracy of the polishing head can be further improved by the use of either estimator. In the calibration layer, OLS and LE have similar capability for predicting and compensating the pose errors. However, in the test layer, LE behaves much better than OLS thanks to its robustness. Table 5 shows that compared with the coarse calibration, the maximum and mean values of the volumetric position/orientation errors of the polishing head can be reduced by as much as 44.6%/55.8% and 57.8%/37.0% when using OLS, whereas the use of LE delivers 66.3%/75.2% and 63.9%/49.3%. Therefore, we can conclude with confidence that LE has a superior capability for predicting and thereby compensating pose errors at any configuration across the task workspace. It is worthwhile stressing again that due to the unmodeled source errors, measurement disturbance, and biased estimation by Liu estimator, the values of the estimated error parameters may differ from their true ones [40, 41]. Nevertheless, the estimate parameters enable the overall discrepancy between the predicted and observed pose errors is minimized, meaning that the discrepancy does not affect the final results of pose error compensation.

Table 3 Estimated parameters by OLS

$\Delta\xi_{a,3,1}$	$\Delta\xi_{a,3,2}$	$\Delta\xi_{a,3,3}$	$\Delta\xi_{a,4,4}$	$\Delta\xi_{a,5,4}$	$\Delta\xi_{a,6,4}$	$\Delta x_{0,1}$	$\Delta y_{0,1}$	$\Delta z_{0,1}$	$\Delta x_{2,1}$	$\Delta z_{2,1}$
4.287	-9.286	-4.380	0.012	0.023	-0.026	-4.098	0.276	2.163	-0.762	2.071
$\Delta z_{3,1}$	$\Delta\alpha_{3,1}$	$\Delta x_{0,2}$	$\Delta y_{0,2}$	$\Delta z_{0,2}$	$\Delta x_{2,2}$	$\Delta z_{2,2}$	$\Delta z_{3,2}$	$\Delta\alpha_{3,2}$	$\Delta x_{6,2}$	$\Delta z_{6,2}$
0.253	0.061	1.906	2.783	1.872	0.443	0.639	0.467	0.072	0.492	-0.517
$\Delta x_{0,3}$	$\Delta y_{0,3}$	$\Delta z_{0,3}$	$\Delta x_{2,3}$	$\Delta z_{2,3}$	$\Delta z_{3,3}$	$\Delta\alpha_{3,3}$	$\Delta x_{6,3}$	$\Delta z_{6,3}$	$\Delta x_{0,4}$	$\Delta y_{0,4}$
-0.472	-4.963	0.173	0.871	-1.319	0.374	0.069	0.375	0.769	-0.175	-3.055
$\Delta z_{0,4}$	$\Delta\alpha_{0,4}$	$\Delta\beta_{0,4}$	$\Delta\gamma_{0,4}$	$\Delta x_{2,4}$	$\Delta z_{2,4}$	$\Delta\alpha_{2,4}$	$\Delta x_{3,4}$	$\Delta z_{3,4}$	$\Delta\alpha_{3,4}$	$\Delta\beta_{3,4}$
1.782	0.112	0.063	-0.107	5.782	0.325	-0.036	0.027	0.012	0.216	-0.462
$\Delta x_{4,4}$	$\Delta y_{4,4}$	$\Delta z_{4,4}$	$\Delta\alpha_{4,4}$	$\Delta\beta_{4,4}$	$\Delta x_{5,4}$	$\Delta z_{5,4}$	$\Delta\alpha_{5,4}$	$\Delta y_{6,4}$	$\Delta\alpha_{6,4}$	
0.207	-2.876	3.879	-0.112	0.204	5.872	2.987	-0.408	3.683	0.309	

length unit: mm, angle unit: deg

Table 4 Estimated parameters by LE

$\Delta\xi_{a,3,1}$	$\Delta\xi_{a,3,2}$	$\Delta\xi_{a,3,3}$	$\Delta\xi_{a,4,4}$	$\Delta\xi_{a,5,4}$	$\Delta\xi_{a,6,4}$	$\Delta x_{0,1}$	$\Delta y_{0,1}$	$\Delta z_{0,1}$	$\Delta x_{2,1}$	$\Delta z_{2,1}$
1.364	-3.259	1.472	-0.020	0.014	0.108	1.982	-2.037	3.162	-0.325	2.485
$\Delta z_{3,1}$	$\Delta\alpha_{3,1}$	$\Delta x_{0,2}$	$\Delta y_{0,2}$	$\Delta z_{0,2}$	$\Delta x_{2,2}$	$\Delta z_{2,2}$	$\Delta z_{3,2}$	$\Delta\alpha_{3,2}$	$\Delta x_{6,2}$	$\Delta z_{6,2}$
-0.367	0.035	2.196	-0.124	0.042	0.381	0.188	0.945	-0.063	2.957	-1.428
$\Delta x_{0,3}$	$\Delta y_{0,3}$	$\Delta z_{0,3}$	$\Delta x_{2,3}$	$\Delta z_{2,3}$	$\Delta z_{3,3}$	$\Delta\alpha_{3,3}$	$\Delta x_{6,3}$	$\Delta z_{6,3}$	$\Delta x_{0,4}$	$\Delta y_{0,4}$
1.423	-0.407	-3.186	1.392	-0.915	0.624	-0.013	-1.376	0.527	-0.279	0.068
$\Delta z_{0,4}$	$\Delta\alpha_{0,4}$	$\Delta\beta_{0,4}$	$\Delta\gamma_{0,4}$	$\Delta x_{2,4}$	$\Delta z_{2,4}$	$\Delta\alpha_{2,4}$	$\Delta x_{3,4}$	$\Delta z_{3,4}$	$\Delta\alpha_{3,4}$	$\Delta\beta_{3,4}$
0.461	0.040	0.028	0.121	2.531	0.615	0.030	0.781	0.284	-0.041	0.074
$\Delta x_{4,4}$	$\Delta y_{4,4}$	$\Delta z_{4,4}$	$\Delta\alpha_{4,4}$	$\Delta\beta_{4,4}$	$\Delta x_{5,4}$	$\Delta z_{5,4}$	$\Delta\alpha_{5,4}$	$\Delta y_{6,4}$	$\Delta\alpha_{6,4}$	
-0.313	0.426	0.881	-0.094	0.051	1.934	1.217	-0.053	-0.210	-0.104	

length unit: mm, angle unit: deg

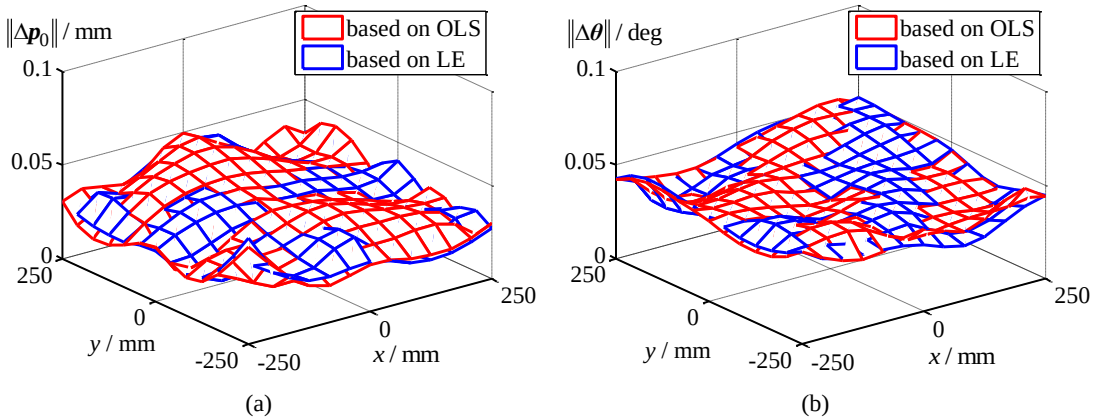

(a) (b)

Fig.8 Pose error distributions in the calibration (lower) layer after the fine calibration (a) position error (b) orientation error.

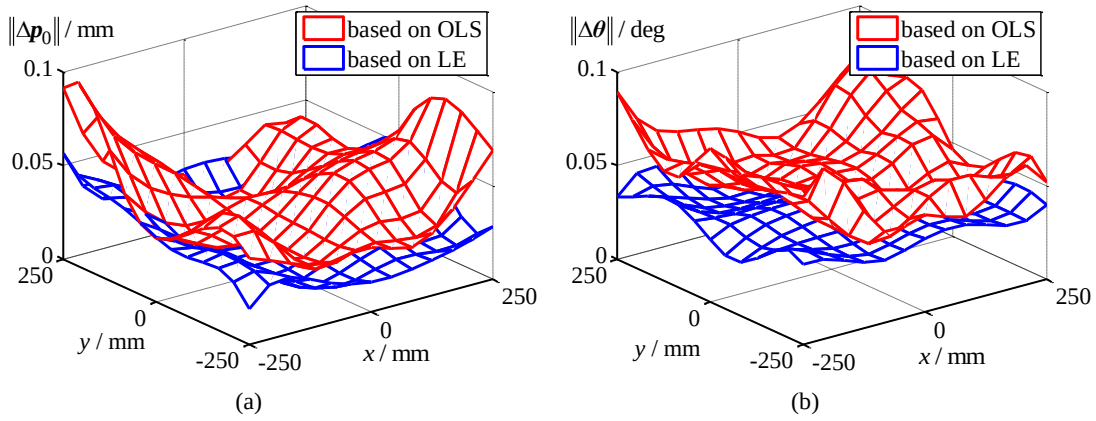

Fig. 9 Pose error distributions in the test (middle) layer after the fine calibration (a) position error (b) orientation error.

Table 5 Pose errors after calibration in three measurement layers

Pose error	Maximum value			Mean value		
	Coarse	OLS	LE	Coarse	OLS	LE
Position/mm	0.166	0.092	0.056	0.083	0.035	0.030
Orientation/deg	0.206	0.091	0.051	0.073	0.046	0.037

6 Conclusions

This paper has proposed and explored a systematic approach for the kinematic calibration of a 6-DOF hybrid robot developed for polishing aspheric lenses. This approach improves the calibration efficiency and accuracy by implementing two successive steps: (1) estimation of the encoder offsets by ordinary least squares (OLS) in an iterative manner until an overall linearized regression model becomes valid; and (2) estimation of the whole set of identifiable error parameters using a Liu estimator on the basis of a column full ranked identification Jacobian reconstructed by correlation analysis. For the prototype machine under investigation, simulation results confirm improved robustness against measurement disturbances by showing that the overall standard deviation of the whole set of identifiable error parameters estimated by LE is 63.9% smaller than that estimated by OLS. Experimental results demonstrate the effectiveness of the approach: following fine calibration the maximum value of the volumetric position and orientation errors of the polishing head can be reduced below 0.06 mm and 0.06 deg by LE in comparison with 0.10 mm and 0.10 deg by OLS throughout a task workspace of $500\ \text{mm}\times 500\ \text{mm}\times 120\ \text{mm}$.

Acknowledgement

This work is partially supported by The National Natural Science Foundation of China (Grants 51420105007, 51605324 and 51721003) and EU H2020-MSCA-RISE 2016 (Grant 734272).

Appendix A

This appendix develops the pose error twist produced by the joint structural errors in a serial kinematic chain, such as shown in Fig. A-1, which might be one limb of a parallel mechanism or an individual system such as a wrist. Without loss of generality, let

$$\boldsymbol{A}_{j,i}=\begin{bmatrix}\boldsymbol{R}_{j,i} & \left[\boldsymbol{r}_{j,i}\times\right]\boldsymbol{R}_{j,i}\\ \boldsymbol{0} & \boldsymbol{R}_{j,i}\end{bmatrix} \tag{A-1}$$

be the 6×6 adjoint transformation matrix, where $\boldsymbol{R}_{j,i}$ denotes the 3×3 orientation matrix of $\{R_{j,i}\}$ with respect to $\{R_0'\}$ and $\left[\boldsymbol{r}_{j,i}\times\right]$ is the 3×3 skew matrix of vector $\boldsymbol{r}_{j,i}$ pointing from P to $A_{j,i}$. The pose error twist produced by the structural errors in the ith limb of the parallel mechanism can be expressed by

$$\$_{g,i}=\sum_{j=j_i}^{n_i}\boldsymbol{A}_{j,i}\Delta\boldsymbol{\eta}_{j,i}=\begin{bmatrix}\boldsymbol{A}_{j_i,i} & \cdots & \boldsymbol{A}_{n_i,i}\end{bmatrix}\begin{pmatrix}\Delta\boldsymbol{\eta}_{j_i,i}\\ \vdots\\ \Delta\boldsymbol{\eta}_{n_i,i}\end{pmatrix}=\boldsymbol{A}_i\Delta\boldsymbol{\eta}_i \tag{A-2}$$

with

$$\Delta\boldsymbol{\eta}_{0,i}=\begin{pmatrix}\Delta x_{0,i} & \Delta y_{0,i} & \Delta z_{0,i} & \Delta\alpha_{0,i} & \Delta\beta_{0,i} & \Delta\gamma_{0,i}\end{pmatrix}^{\mathrm{T}}$$

$$\Delta\boldsymbol{\eta}_{j,i}=\begin{pmatrix}\Delta x_{j,i} & \Delta y_{j,i} & (1-k)\Delta z_{j,i} & \Delta\alpha_{j,i} & \Delta\beta_{j,i} & k\Delta\gamma_{j,i}\end{pmatrix}^{\mathrm{T}},\ k=\begin{cases}0 & \text{R joint}\\ 1 & \text{P joint}\end{cases}$$

where $\Delta x_{j,i}$, $\Delta y_{j,i}$ and $\Delta z_{j,i}$ ($\Delta\alpha_{j,i}$, $\Delta\beta_{j,i}$ and $\Delta\gamma_{j,i}$) denote the structural errors along (about) the $x_{j,i}$, $y_{j,i}$ and $z_{j,i}$ axes of $\{R_{j,i}\}$, except for the one along (about) a joint axis. For the hybrid polishing robot being considered, $j_i=0,\ n_1=n_2=n_3=6$ for the UPS limbs, and $j_i=0, n_4=3$ for the UP limb of the parallel mechanism, giving

$$\boldsymbol{G}_{Pa}=\mathrm{diag}\left[\hat{\$}_{wa,3,i}^{\mathrm{T}}\boldsymbol{A}_i\right],\ \Delta\boldsymbol{\eta}_{Pa}=\begin{pmatrix}\Delta\boldsymbol{\eta}_1^{\mathrm{T}} & \Delta\boldsymbol{\eta}_2^{\mathrm{T}} & \Delta\boldsymbol{\eta}_3^{\mathrm{T}}\end{pmatrix}^{\mathrm{T}} \tag{A-3}$$

$$\boldsymbol{G}_{Pc}=\begin{bmatrix}\hat{\$}_{wc,1,4} & \hat{\$}_{wc,2,4} & \hat{\$}_{wc,3,4}\end{bmatrix}^{\mathrm{T}}\boldsymbol{A}_4,\ \Delta\boldsymbol{\eta}_{Pc}=\Delta\boldsymbol{\eta}_4 \tag{A-4}$$

whereas $j_i=4$, $n_4=6$ for the wrist, so that

$$\boldsymbol{G}_S=\begin{bmatrix}\boldsymbol{A}_{4,4} & \boldsymbol{A}_{5,4} & \boldsymbol{A}_{6,4}\end{bmatrix},\Delta\boldsymbol{\eta}_S=\begin{pmatrix}\Delta\boldsymbol{\eta}_{4,4}^{\mathrm{T}} & \Delta\boldsymbol{\eta}_{5,4}^{\mathrm{T}} & \Delta\boldsymbol{\eta}_{6,4}^{\mathrm{T}}\end{pmatrix}^{\mathrm{T}} \tag{A-5}$$

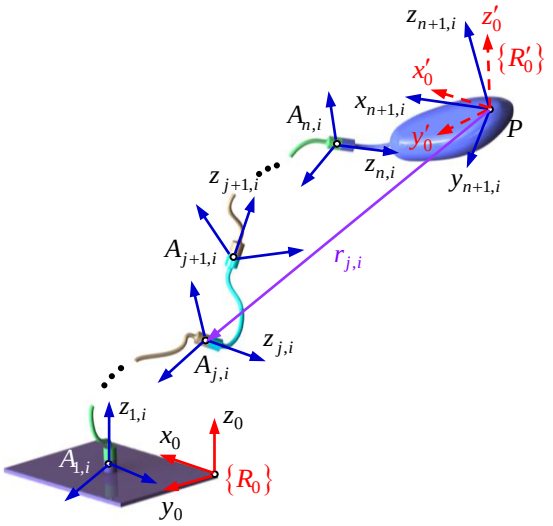

Fig. A-1 Establishment of frames on a serial kinematic chain.

References

[1] W. Rupp, Conventional optical polishing techniques, Int. J. Optics 18(1) (1971) 1-16.

[2] Y. Kakinuma, K. Igarashi, S. Katsura, T. Aoyama, Development of 5-axis polishing machine capable of simultaneous trajectory, posture, and force control, Ann. CIRP 62(1) (2013) 379-382.

[3] C. Fan, G. Zhao, J. Zhao, L. Zhang, L. Sun, Calibration of a parallel mechanism in a serial-parallel polishing machine tool based on genetic algorithm, Int. J. Adv. Manuf. Tech. 81(1) (2015) 1-11.

[4] Z. Li, P. Xu, J. Zhang, B. Li, Z. Zhang, Design of high-precision contour control system for a polishing mechanism, Chin. J. Sci. Instrum. 36 (2015) 330-337.

[5] M. Weck, D. Staimer, Parallel kinematic machine tools – current state and future potentials, Ann. CIRP 51(2) (2002) 671-683.

[6] R. Ramesh, M. Mannan, A. Poo, Error compensation in machine tools — a review: Part I: geometric, cutting-force induced and fixture-dependent errors, Int. J. Mach. Tools Manu. 40(9) (2000) 1235-1256.

[7] R. Ramesh, M. Mannan, A. Poo, Error compensation in machine tools—a review: Part II: thermal errors, Int. J. Mach. Tools Manu. 40(9) (2000) 1257-1284.

[8] M. Verner, F. Xi, C. Mechefske, Optimal calibration of parallel kinematic machines, J. Mech. Design. 127 (7) (2005) 62–69.

[9] X. Ren, Z. Feng, C. Su, A new calibration method for parallel kinematics machine tools using orientation constraint, Int. J. Mach. Tools Manu. 49(9) (2009) 708-721.

[10] J. Fu, F. Gao, W. Chen, Y. Pan, R. Lin, Kinematic accuracy research of a novel six-degree-of-freedom parallel robot with three legs, Mech. Mach. Theory, 102 (2016) 86-102.

[11] T. Sun, Y. Zhai, Y. Song, J. Zhang, Kinematic calibration of a 3-DOF rotational parallel manipulator using laser tracker, Robot. Com.-Int. Manuf. 41 (2016) 78-91.

[12] P. Huang, J. Wang, L. Wang, R. Yao, Kinematical calibration of a hybrid machine tool with regularization method, Int. J. Mach. Tools Manu. 51(3) (2011) 210-220.

[13] M. Neubauer, H. Gattringer, A. Müller, A. Steinhauser, W Höbarth, A two-stage calibration method for industrial robots with joint and drive flexibilities, Mech. Sci. 6(2) (2015) 191-201.

[14] N. Nguyen, J. Zhou, H. Kang, A calibration method for enhancing robot accuracy through integration of an extended Kalman filter algorithm and an artificial neural network, Neurocomputing, 151 (2015) 996-1005.
[15] H. Zhuang, J. Wu, W. Huang, Optimal planning of robot calibration experiments by genetic algorithms, IEEE International Conference on Robotics and Automation, Minneapolis, USA, (1996) 981-986.
[16] T. Li, K. Sun, Y. Jin, H. Liu, A novel optimal calibration algorithm on a dexterous 6 DOF serial robot with the optimization of measurement poses number, IEEE International Conference on Robotics and Automation, Shanghai, China, (2011) 975-981.
[17] A. Joubair, A. Bonev, Comparison of the efficiency of five observability indices for robot calibration, Mech. Mach. Theory, 70(6) (2013) 254-265.
[18] J. Zhou, N. Nguyen, H. Kang, Selecting optimal measurement poses for kinematic calibration of industrial robots, Adv. Mech. Eng. 8(1) (2014) 1-9.
[19] T. Gayral, D. Daney, A sufficient condition for parameter identifiability in robotic calibration, Mech. Mach. Sci. 15(1) (2014) 131-138.
[20] W. Tian, F. Yin, H. Liu, J. Li, Q. Li, T. Huang, D. Chetwynd, Kinematic calibration of a 3-DOF spindle head using a double ball bar, Mech. Mach. Theory, 102 (2016) 167-178.
[21] P. Chang, J. Wang, T. Li, X. Liu, L. Guan, Step kinematic calibration of a 3-DOF planar parallel kinematic machine tool, Sci. China Ser. E, 51(12) (2008) 2165-2177.
[22] C. Escande, T. Chettibi, R. Merzouki, V. Coelen, P. Pathak, Kinematic calibration of a multisection bionic manipulator, IEEE-ASME T. Mech. 20(2) (2015) 663-674.
[23] P. Bai, J. Mei, T. Huang, D. Chetwynd, Kinematic calibration of Delta robot using distance measurements, P. I. Mech. Eng. C-J. Mec. 230(3) (2016) 414-424.
[24] R. He, Y. Zhao, S. Yang, S. Yang, Kinematic parameter identification for serial-robot calibration based on POE formula, IEEE T. Robot. 26(3) (2010) 411-423.
[25] G. Chen, H. Wang, Z. Lin, Determination of the identifiable parameters in robot calibration based on the POE formula, IEEE T. Robot. 30(5) (2014) 1066-1077.
[26] G. Chen, L. Kong, Q. Li, H. Wang, Z. Lin. Complete, minimal and continuous error models for the kinematic calibration of parallel manipulators based on POE formula, Mech. Mach. Theory, 121 (2018) 844-856.
[27] N. Boari, F. Gagliardi, P. Castellazzi, P. Mortini, Identification and observability measure of a basis set of error parameters in robot calibration, J. Mech. Design, 111(4) (1989) 513-518.
[28] J. Hollerbach, C. Wampler, The calibration index and taxonomy for robot kinematic calibration methods, Int. J. Robot. Res. 15(6) (1996) 573-591.
[29] U. Dolinsky, D. Jenkinson, J. Colquhoun, Application of genetic programming to the calibration of industrial robots, Comput. Ind. 58(3) (2007) 255-264.
[30] Z. Jiang, W. Zhou, H. Li, Y. Mo, W. Ni, Q. Huang, A new kind of accurate calibration method for robotic kinematic parameters based on extended Kalman and particle filter algorithm, IEEE T. Ind. Electron. 65(4) (2018) 3337-3345.
[31] C. Stein, Inadmissibility of the usual estimator for the mean of a multivariate normal distribution, Berkeley Symposium on Mathematical Statistics & Probability, Berkeley, USA, (1955) 197-206.
[32] A. Hoerl, R. Kennard, Ridge regression: biased estimation for nonorthogonal problems, Technometrics, 12(1) (1970) 55-67.
[33] W. Massy, Principal components regression in exploratory statistical research, Publ. Am. Stat. Assoc. 60(309) (1965) 234-256.
[34] K. Liu, A new class of biased estimate in linear regression, Commun. Stat. 22(2) (1993) 393-402.
[35] K. Liu, Using Liu-type estimator to combat collinearity, Commun. Stat. - Theor. M. 32(5) (2003) 1009-1020.
[36] A. Duran, F. Akdeniz, H. Hu, Efficiency of a Liu-type estimator in semiparametric regression models, J. Comput. Appl. Math. 235(5) (2011) 1418-1428.
[37] D.B. Erdogan, Liu-type logistic estimator, Commun. Stat. – Simul. C. 42(7) (2013) 1578-1586.
[38] H. Liu, T. Huang, D. Chetwynd, A general approach for geometric error modeling of lower mobility parallel manipulators, J. Mech. Robot. 3(2) (2011) 686-697.
[39] T. Huang, D. Chetwynd, D. Whitehouse, J. Wang, A general and novel approach for parameter identification of 6-DOF parallel kinematic machines, Mech. Mach. Theory. 40(2) (2005) 219-239.
[40] C. Douglas, A. Elizabeth, V. Geoffrey, Introduction to linear regression analysis 5th ed, Wiley, New Jersey, USA, (2011).
[41] B. Mooring, Z. Roth, M. Driels, Fundamentals of manipulator calibration, Wiley, New Jersey, USA, (1991).
[42] B. Institution, Manipulating industrial robots – performance criteria and related test methods, International Standards Organization (1998).